Biomimetic Nonlinear X-Shaped Vibration Isolation System for Jacket Offshore Platforms

Zhenghan Zhu and Yangmin Li *

Posted Date: 7 October 2025

doi: 10.20944/preprints202510.0385.v1

Keywords: passive vibration isolation; nonlinear stiffness; offshore jacket platform; X-shaped mechanism; Quasi-zero stiffness

 doi:10.20944/preprints202510.0385.v1

Article

Biomimetic Nonlinear X-Shaped Vibration Isolation System for Jacket Offshore Platforms

Zhenghan Zhu and Yangmin Li *

Department of Industrial and Systems Engineering, The Hong Kong Polytechnic University, Hong Kong SAR 999077, China

* Correspondence: yangmin.li@polyu.edu.hk

Abstract

Vibrations induced by marine environmental loads can compromise the operational performance of offshore platforms and, in severe cases, result in structural instability or overturning. This study proposes a biomimetic nonlinear X-shaped vibration isolation system (NXVIS) to suppress earthquake-induced vibration response in offshore platforms. Compared with traditional passive vibration isolators, the key innovations of the NXVIS include: (1) the proposed NXVIS can be tailored to different load requirements and resonant frequencies to accommodate diverse offshore platforms and environmental loads; (2) By adjusting isolator parameters (e.g., link length and spring stiffness, etc.), the anti-vibration system can achieve different types of nonlinear stiffness and a large-stroke quasi-zero stiffness (QZS) range, enabling ultra-low frequency (ULF) vibration control without compromising load capacity. To evaluate the effectiveness of the designed NXVIS for the vibration suppression of jacket offshore platforms under seismic loads, numerical analysis was performed on a real offshore platform and seismic loads. The results show that the proposed nonlinear vibration isolation solution significantly reduces the dynamic response of deck displacement and acceleration under seismic loads, demonstrating effective low-frequency vibration control. This proposed NXVIS provides a novel and effective method for manipulating beneficial nonlinearities to achieve improved anti-vibration performance.

Keywords: passive vibration isolation; nonlinear stiffness; offshore jacket platform; X-shaped mechanism; Quasi-zero stiffness

1. Introduction

Jacket platforms are fixed platforms secured to the seabed by steel piles penetrating a certain depth, which are widely used in offshore oil and gas production. Due to structural characteristics and operating environment, jacket platforms are susceptible to various marine environmental loads, such as earthquakes, wind, waves, ice loads, and ship impacts. Long-term exposure to these marine environments can cause structural vibrations of jacket platforms, which can cause fatigue damage to the steel structure, impacting platform production efficiency and even leading to catastrophic failure [1,2]. Furthermore, external disturbances inevitably affect worker productivity and comfort, negatively impacting production cost control. Extensive research has been conducted on vibration control of jacket platforms under marine environmental loads [3]. However, most efforts have focused on suppressing vibrations caused by wave excitation, while limited research has considered seismic excitation [4–6]. This is because waves are the most common loads on offshore platforms, constantly impacting structural stability [3,7]. However, structural damage caused by waves is long-term, and the initial site selection of offshore platforms usually considers local hydrological conditions. Therefore, limit wave loads can cause irreversible damage to the platform in a single instance. However, seismic loads are unpredictable and have a wide frequency range (mostly concentrated between 0.7 and 3.0 Hz) [8,9]. Strong earthquakes often have catastrophic effects on

 doi:10.20944/preprints202510.0385.v1

offshore platforms and can cause severe damage to these structures [5,6,10,11]. Furthermore, the first-order vibration mode of most offshore platform falls within the frequency range of seismic energy [4,12], which can trigger resonance in the offshore platform and amplify the destructive power of the earthquake. Statistics indicate that approximately hundreds of offshore platforms are currently located in seismically active areas [5]. Therefore, studying the vibration control of jacket offshore platforms under seismic loads is of great significance.

The jacket offshore platform exhibits a low fundamental natural frequency and a high modal density in its vibrational characteristics. The overall structure has strong coupling and nonlinearity, and the external load has uncertainty, making offshore platform vibration control a very challenging problem [3,12]. Active and semi-active control are not suitable for long-term vibration control of large structures such as offshore platforms due to their high energy consumption and the need for accurate models of the controlled objects [2,12]. Passive control is the earliest and most widely used vibration control method due to reliability, low cost, and the advantages of no electronic equipment. Passive control achieves the purpose of vibration reduction by arranging absorption, dissipation or vibration isolation devices in the target structure and utilizing the characteristics of the device itself [3,13,14]. Dissipation mothed primarily utilizes the energy dissipation mechanism of the damping structure, i.e., by irreversibly converting the mechanical energy (kinetic and potential energy) that causes vibration into other forms of energy (primarily heat) and dissipating it, thereby suppressing the vibration response. For example, Mostafa Vaezi et al. [15] numerically simulated jacket offshore platforms with various distributions and three different support-viscous damper system configurations (knuckle, herringbone, and diagonal configurations) and various support stiffnesses under irregular wave loads, and proposed a spatially optimized layout for the support-viscous damper system. Jiang et al. [16] investigated the effectiveness of viscous dampers (VDs) in reducing vibration on offshore platforms under the combined effects of wind, waves, and earthquakes. The results showed that VDs placed diagonally at each structural level can effectively suppress platform vibration under both isolated earthquakes and wind-wave-earthquake conditions. According to their research results, passive control systems based on these devices are effective for offshore platforms under wave loads. Absorption method is the dominant approach in passive vibration control on offshore platforms. Its core principle is to attach a substructure (a mass-spring-damper system) and tune its frequency to the natural frequency of the main structure, absorbing the main structure's vibration energy through anti-phase motion. For example, Cui et al. [17] applied tuned liquid multi-column damper (TLMCD) to the columns of tension leg platforms (TLP) to attenuate the heave response of TLP. Ghasemi et al. [18] used shape memory alloy pounding tuned mass damper (SMA-PTMD) to control the wave-induced vibration of jacket offshore platforms. The results showed that SMA-PTMD can effectively reduce the displacement response of the platform deck. Liu et al. [19] investigated the dynamic response of jacket offshore platforms under the action of wave and seismic excitation using multiple tuned mass dampers (MTMDs), considering the influence of soil-structure interaction (SSI). Furthermore, the core concept of isolation method is to insert a "flexible layer" (i.e., an isolation system) between the vibration source (e.g., waves, earthquakes) and the objective structure to be protected (e.g., platform deck, equipment). This modifies the dynamic characteristics of system, thereby reducing the transfer of vibration energy. It also shifts the system's natural frequency away from the frequencies of major environmental loads (such as earthquakes and waves), avoiding resonance. For example, Ou et al. [11] employed a rubber vibration isolation system to reduce the vibration response of jacket offshore platforms under wave loads. The isolation system consists of passive dampers, which primarily dissipate vibration energy through their damping properties. However, these passive control devices are designed based on the characteristics of the structure or specific excitation and can only perform optimally at a certain frequency ratio. That is, they cannot work properly when the dynamic characteristics of the structure or load change [3,20]. The frequency band of earthquakes is relatively wide, and existing passive control facilities cannot achieve ideal vibration control. In summary, it is very important to develop a passive vibration

 doi:10.20944/preprints202510.0385.v1

control method that can be customized according to different load requirements and resonant frequencies, is basically maintenance-free, and is effective across the entire seismic frequency range.

In recent years, passive vibration isolators, developed by leveraging the advantages of nonlinearity, may offer an effective solution. Traditional linear passive vibration isolators cannot resolve the contradiction between low-frequency vibration isolation and load-bearing capacity [21]. To isolate low-frequency vibrations, it is necessary to reduce stiffness; however, soft springs exhibit large static deformations and suffer from poor static stability and load-bearing capacity. An ideal vibration isolation system should meet the requirements of low-frequency and broad-band frequency vibration suppression without reducing the system's load-bearing capacity [22]. Nonlinear passive vibration isolation systems represent a significant advancement in the field, marking a transition from static, fixed-performance technologies toward dynamic and adaptively capable solutions. Through ingenious mechanical design, these systems achieve nonlinear dynamic characteristics that lead to breakthrough performance, particularly in addressing challenges such as ULF vibration isolation and high load-bearing/counter-impact capacity [23–25]. To this end, many novel structures or control methods have been proposed to improve vibration isolation performance, such as quasi-zero structures, compliant mechanisms based quasi zero stiffness isolator, origami structures, smart materials and bionic X-shaped mechanisms [18,25–29]. Among them, the bionic NXVIS has received widespread attention. This method is inspired by the vibration-suppressing properties of animal legs/limbs. Jing's research team has developed a large number of simulated nonlinear X-shaped anti-vibration methods and conducted in-depth research on nonlinear stiffness, damping, and inertia, proving the reliability of the NXVIS [22]. Due to its excellent nonlinear adjustable characteristics, it enables the design of passive isolators that combine low dynamic stiffness with high load-bearing capacity, achieving tunable ULF and broadband vibration suppression [21,22]. In addition, the nonlinear damping in the system can achieve energy dissipation, further reducing the amplitude of structural vibration. It is well known that the deck layer is the part with the most concentrated mass of the offshore platform and is also an important place for oil and gas production and workers' living [30]. The nonlinear characteristics of the NXVIS mean that the isolation system can achieve ULF and broadband vibration suppression under seismic loads while ensuring the stability of the deck layer. However, there are no published reports on the results of using the biomimetic NXVIS for offshore platform vibration control under seismic excitation.

In summary, this paper develops a biomimetic NXVIS for vibration control of jacket offshore platforms under seismic loads. Through theoretical research and numerical simulation under real marine conditions, the effectiveness of the proposed NXVIS for vibration control of jacket offshore platforms under seismic loads is systematically discussed. The second part of this paper formulates a mathematical model of the NXVIS, introduces its load-bearing capacity and adjustable nonlinear characteristics, and verifies its ULF and broad-band frequency vibration isolation performance. The third part introduces the structure and characteristics of the NRB' jacket platform and formulates a dynamic model of the offshore platform equipped with the NXVIS. The fourth part discusses the anti-vibration performance of the NRB' platform based on the NXVIS using two typical seismic loads as an example. Finally, a summary of the entire paper is given.

2. Biomimetic Nonlinear X-Shaped Anti-Vibration Mechanism

2.1. Modeling of the X-Shaped Anti-Vibration Mechanism

Drawing inspiration from the exceptional vibration suppression mechanisms inherent to biological systems, this research introduces an innovative biomimetic isolation strategy specifically designed for jacket offshore platforms. This method can obtain superior ULF vibration isolation and superior anti-vibration performance across a wide frequency range. A schematic layout of the proposed bio-inspired NXVIS is shown in Figure 1. The isolation structure consists of an X-shaped support leg to simulate human knee bending and a spring-damper system to simulate leg muscles.

 doi:10.20944/preprints202510.0385.v1

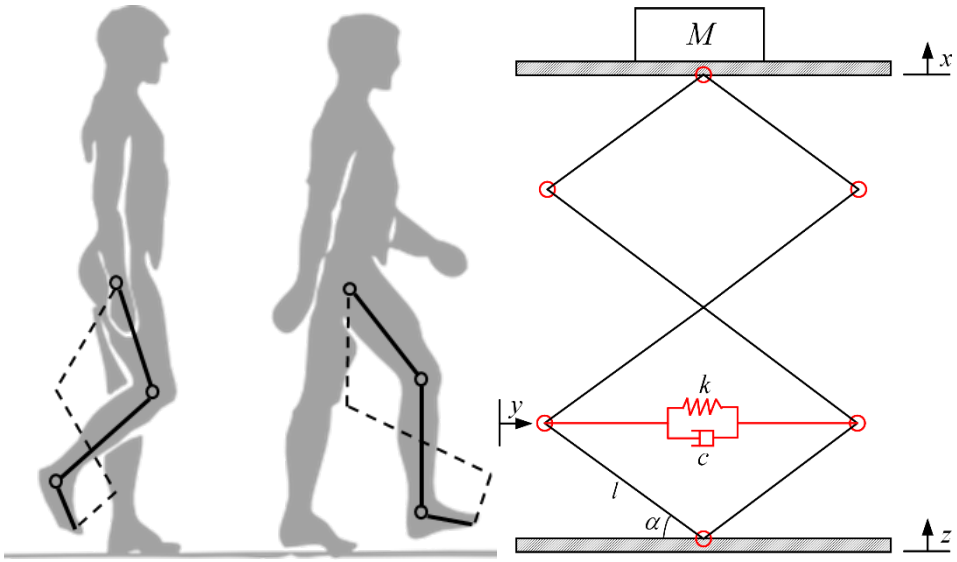

(a)Legs motion during walking. (b) X-shaped isolator.

Figure 1. The biomimetic NXVIS.

As shown in Figure 1, the biomimetic NXVIS (Figure 1b) draws inspiration from the biomechanical configuration of the human leg during gait, with clearly labeled structural parameters. The target vibration isolation layer M is supported by the X-shaped structure. The bar length and initial installation angle of the X-shaped structure are l and α, respectively. The displacements of the top layer and the ground are x and z, respectively. A spring and damper are placed at the bottom of the NXVIS, with their stiffness and damping coefficients being k and c, respectively. Findings from the literature confirm the capability of the X-shaped isolator to achieve high static stiffness concurrently with low dynamic stiffness [21].

Due to the relative motion between the target layer and the base layer, geometric changes will occur between the NXVIS, as shown in Figure 2. Note that n is the number of layers in the X-shaped vibration isolation structure.

The spring extension y can be written as,

$$y = 2l\cos\alpha - 2\sqrt{l^2 - \left(l\sin\alpha + \hat{x}/2n\right)^2} \tag{1}$$

where, $\hat{x} = x - z$.

According to the above geometric relationship and Lagrange principle, the dynamic equation of the X-shaped anti-vibration mechanism is as follows,

$$M\ddot{x} + k\left(y - y_s\right)\frac{\partial y}{\partial \hat{x}}\frac{\partial \hat{x}}{\partial x} + Mg = -c\frac{\partial y}{\partial \hat{x}}\frac{\partial \hat{x}}{\partial t} \tag{2}$$

where, y_s is the extension of the spring due to the weight of the loading M, which can be written as,

$$y_s = 2\sqrt{l^2 - \left(l\sin\beta - \hat{x}/2n\right)^2} - 2l\cos\beta \tag{3}$$

where, β is the angle between the isolator and the ground when the spring is in its original length and not subject to load M. The detailed calculation process of the dynamic equation can be found in Reference [22].

 doi:10.20944/preprints202510.0385.v1

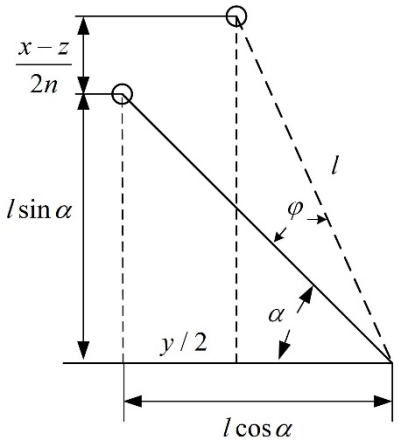

Figure 2. Dynamic changes in geometric relationships.

For the convenience of calculation, the stiffness term and damping term in Equation (2) are Taylor expanded at $\hat{x}=0$, which can be expressed as,

$$T_1=(y-y_s)\frac{\partial y}{\partial \hat{x}}\frac{\partial \hat{x}}{\partial x}=\varepsilon_0+\varepsilon_1\hat{x}+\varepsilon_2\hat{x}^2+\varepsilon_3\hat{x}^3 \quad (4)$$

$$T_2=c\frac{\partial y}{\partial \hat{x}}\frac{\partial \hat{x}}{\partial t}=\varepsilon_4+\varepsilon_5\hat{x}+\varepsilon_6\hat{x}^2+\varepsilon_7\hat{x}^3 \quad (5)$$

where the coefficients $\varepsilon_0-\varepsilon_7$ are listed in the "Appendix B". The accuracy of the Taylor expansion was evaluated by comparing the approximated terms (T_1, T_2) with the exact stiffness and damping terms within the specified working range (parameters provided in "Appendix A"). The comparative outcomes are summarized in Figure 3.

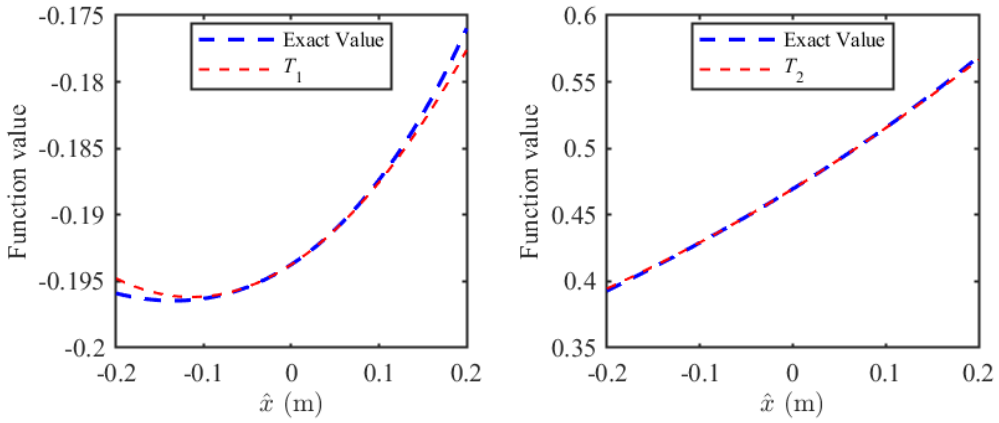

Figure 3. The comparison between the exact value and the approximated value.

As can be seen from Figure 3, the approximate value obtained by Taylor expansions has a good match with the exact value within the given motion range up to ±2m, which is enough for the following vibration analysis. Therefore, the dynamic motion can be simplified as,

$$M\ddot{x}+cT_2+kT_1+Mg=-M\ddot{z} \quad (6)$$

2.2. Static Stiffness Analysis

To reduce vibration transmission, the stiffness of traditional vibration isolation systems is often adjusted to a very small value, which will reduce the load capacity of the structure and even risk collapse. The NXVIS proposed in this paper has good high static and low dynamic stiffness (HSLDS) characteristics, ensuring that the structure has sufficient load capacity while minimizing vibration transmission. To verify the HSLDS characteristics of the proposed NXVIS, static force analysis is very

 doi:10.20944/preprints202510.0385.v1

necessary. The functional dependence of the load force F_s on the relative displacement $\hat{x}$ is expressed as,

$$F_s = \frac{1}{2} k y_s \frac{l \sin\beta - \hat{x}/2n}{y_s/2 + l\cos\beta} \tag{7}$$

The conclusions drawn from the non-dimensional form no longer rely on a specific spring size or stiffness. As long as the non-dimensional parameters are the same, similar structures of any size will exhibit exactly the same non-dimensional force-displacement curve. Thus, the nonlinear static force is nondimensionalized and written as,

$$F_{Non} = F_s/(kl) = \frac{1}{2} y_s \frac{\sin\beta - \frac{\hat{x}}{l}/2n}{y_s/2 + l\cos\beta} = \frac{1}{2} y_s \frac{\sin\beta - X_{Non}/2n}{y_s/2 + l\cos\beta} \tag{8}$$

Where, the non-dimensional static force and the non-dimensional displacement are $F_{Non} = F_s/kl$ and $X_{Non} = \hat{x}/l$.

According to Equation (8) and Appendix A, the non-dimensional static force-displacement curve of the proposed NXVIS is shown in Figure 4.

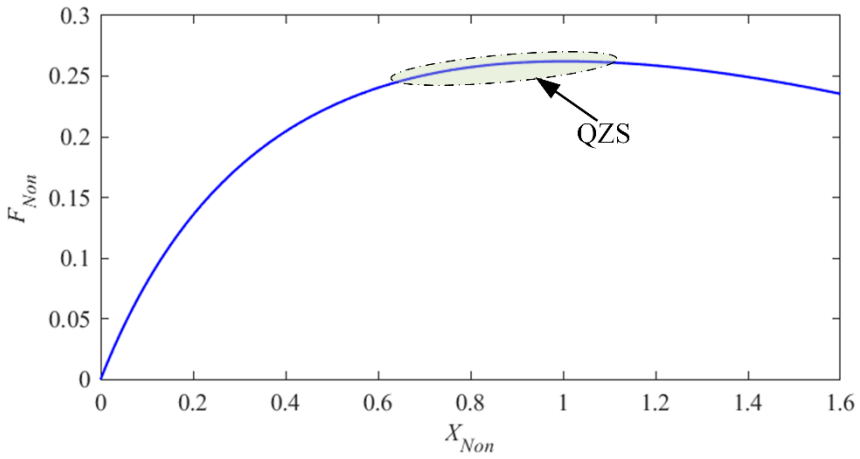

Figure 4. Non-dimensional static force-displacement curve.

Figure 4 depicts the nonlinear relationship between the non-dimensional static load F_{Non} and the non-dimensional displacement X_{Non}. As X_{Non} increases, F_{Non} also increases, but its slope (non-dimensional static stiffness) decreases, gradually achieving quasi-zero stiffness (QZS). QZS creates a region of near-zero dynamic stiffness near the static equilibrium point, thereby resolving the fundamental challenge of traditional linear isolators in achieving both high-load and low-frequency vibration isolation. However, for vibration isolation systems, the static equilibrium position should be located within the positive stiffness range, and negative stiffness should not exist within the vibration range of the target layer. This is because negative stiffness can cause the isolator to collapse, leading to failure of the isolation system. Based on these considerations, this paper defines an indicator for evaluating the QZS: when the ratio of the non-dimensional static force F_{Non} to the non-dimensional displacement X_{Non}—the non-dimensional structural stiffness K_{Non}—is less than 0.007, the corresponding region is defined as the QZS. As shown in Figure 4, when $X_{Non} = 0.7$, the system enters the QZS region, where the non-dimensional stiffness approaches zero, which is ideal for vibration isolation. Considering the mass of the offshore platform deck and the definition of QZS, the angle between the isolator and the ground is set to the angle when $X_{Non} = 0.7$. Furthermore, when $X_{Non} = 0.7$, the load capacity of single X-shaped isolator is 1.94×10^7 N. To meet the design requirement (the target deck mass is 3.1×10^4 tons), the number of X-shaped isolators in the X-shaped vibration isolation layer should be set to 16.

 doi:10.20944/preprints202510.0385.v1

2.3. Parametric Analysis

According to Equations (4) and (5), the nonlinear forces arise from a coefficient set {T_1, T_2}, where T_1 defines the stiffness force and T_2 the damping force. Both of these coefficients are governed by the common isolator parameters l, α, and n. To further understand the impact of structural parameters on the system's nonlinearity, a parameter analysis was performed. It was assumed that when one parameter is varied, the others remain constant.

The nonlinear stiffness coefficient T_1 and the nonlinear damping coefficient T_2 versus displacement $\hat{x}$ for bar length l ranging from 0.60 m to 0.90 m is shown in Figure 5. It can be seen that the stiffness coefficient T_1 and the damping coefficient T_2 are constant at $\hat{x}$ = 0. As bar length l increases, the stiffness coefficient T_1 gradually decreases in the compression range and increases in the extension range. The nonlinearity is strongest when bar length l is small. The damping coefficient T_2 exhibits an opposite relationship with bar length l as the stiffness coefficient T_1.

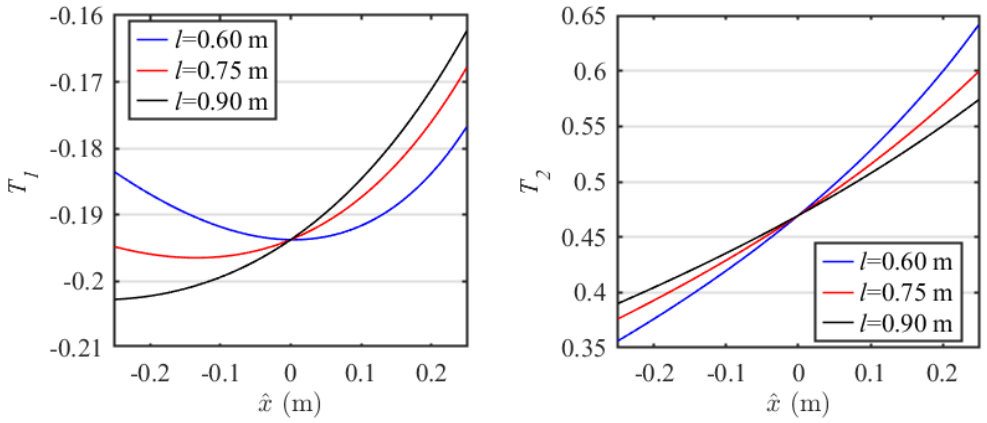

(a) Stiffness coefficient, (b) Damping coefficient.

Figure 5. The coefficient value with different bar length l.

Figure 6 shows the nonlinear stiffness coefficient T_1 and nonlinear damping coefficient T_2 versus displacement $\hat{x}$, as the initial installation angle α changes from 43° to 48°. As can be seen, both the value and nonlinearity of the nonlinear stiffness coefficient T_1 increase with decreasing angle α. This is because a smaller initial installation angle α brings the NXVIS closer to the quasi-zero range, resulting in smaller stiffness. The relationship between the nonlinear damping coefficient T_2 and the initial installation angle α is opposite to that of the nonlinear stiffness coefficient T_1.

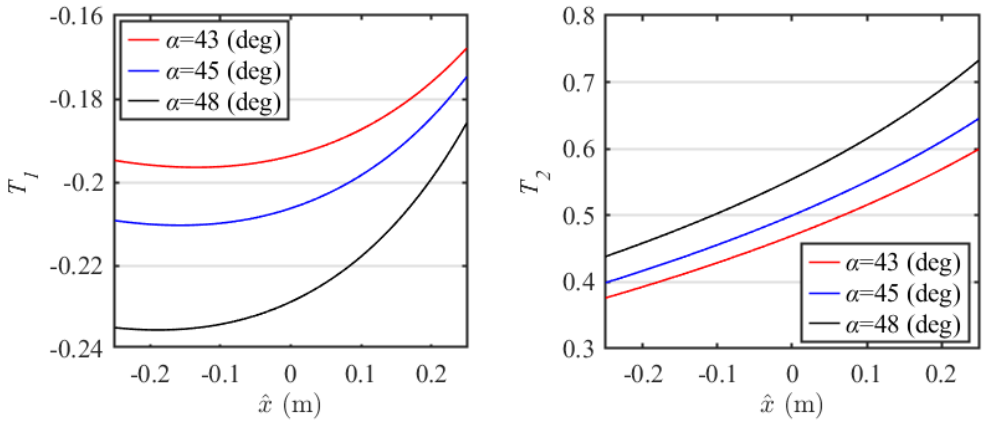

(a) Stiffness coefficient, (b) Damping coefficient.

Figure 6. The coefficient value with different angle α.

 doi:10.20944/preprints202510.0385.v1

The number of layers n of the NXVIS changes from 2 to 4, and the nonlinear stiffness coefficient T_1 and the nonlinear damping coefficient T_2 with respect to the displacement $\hat{x}$ are shown in Figure 7. It can be seen that with the increase of the number of layers n, the value of coefficient T_1 rises significantly, but the nonlinearity decreases. The nonlinear damping coefficient T_2 exhibits an opposite relationship to the nonlinear stiffness coefficient T_1, but the rate of change is increasing with decreasing layer number n.

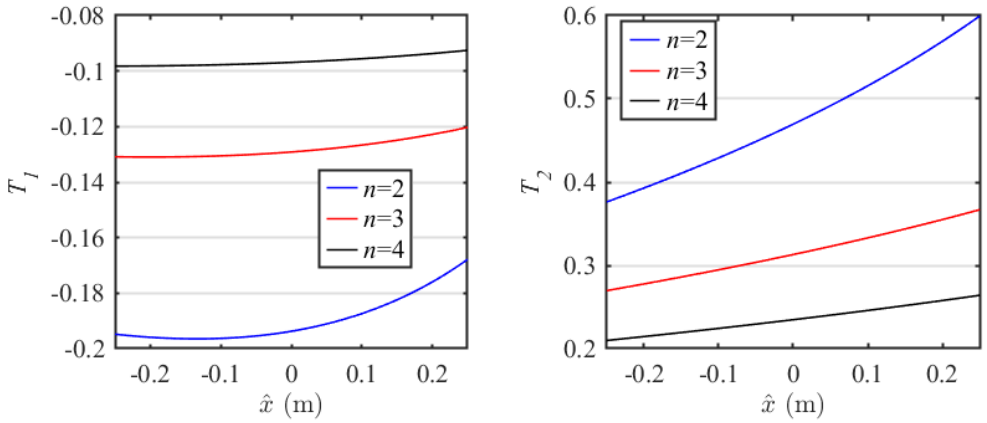

(a) Stiffness coefficient, (b) Damping coefficient.

Figure 7. The coefficient value with different layer number n.

From Figures 5–7, it can be concluded that changes in the bar length l, initial installation angle α, and number of layers n can all lead to corresponding changes in the nonlinear stiffness coefficient T_1 and the nonlinear damping coefficient T_2. In particular, the bar length l causes the nonlinear stiffness coefficient T_1 to produce significant nonlinear characteristics, which is conducive to optimizing stiffness. This also shows that parameter adjustments of the NXVIS will produce a special dynamic response under external excitation, thereby achieving a better passive vibration isolation effect by optimizing the structural parameters. An ideal vibration isolation system requires low stiffness and appropriate damping while ensuring sufficient load capacity.

2.4. Displacement Transmissibility

To evaluate and verify the anti-vibration performance of the proposed NXVIS, the harmonic balance method is adopted to obtain the transmissibility of the system. According to the dynamic Equation (6), it is assumed that the base excitation is expressed as,

$$z = z_0 \cos(\omega t + \sigma) \quad (9)$$

where, z_0, ω and σ are the amplitude, frequency and initial phase of the excitation signal respectively.

The solution of the dynamic equation is assumed as,

$$\hat{x} = x_0 \cos(\omega t) \quad (10)$$

where, x_0 and σ are the motion amplitude and amplitude. The σ and x_0 in Equations (9) and (10) can be determined using the following equations,

$$c\varepsilon_3 a + \frac{1}{4} c\varepsilon_5 a^3 = \omega M z_0 \sin\sigma \quad (11)$$

$$k\varepsilon_1 a - \omega^2 M a = \omega^2 M z_0 \cos\sigma \quad (12)$$

Based on Equations (11) and (12), the value of σ and x_0 can be derived. So, the displacement transmissibility T_d can be obtained by,

 doi:10.20944/preprints202510.0385.v1

$$T_d = 20\lg\left|\frac{\sqrt{a^2 + 2az_0\cos\psi + z_0^2}}{z_0}\right| \quad (13)$$

Based on the parameters in "Appendix A" and Equation (13), the transmissibility of the NXVIS is shown in Figure 8.

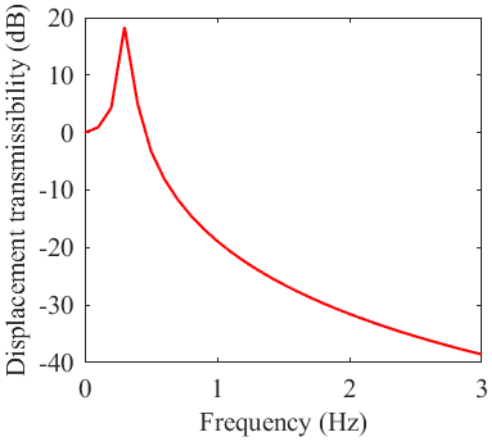

Figure 8. The displacement transmissibility of the proposed NXVIS.

Earthquakes are generally considered to be a predominantly low-frequency excitation. While the energy released by an earthquake encompasses a wide frequency range, its frequency distribution shows that the vast majority is concentrated between 0.7 Hz and 3.0 Hz [12]. This is the primary cause of severe damage to high-rise buildings and long-period structures (such as jacket platforms, suspension bridges and supertall buildings) during large earthquakes. Figure 8 shows that the system's resonant frequency is 0.3 Hz. Once the frequency surpasses 0.4 Hz, the system transitions into its vibration attenuation zone, confirming the proposed isolation mechanism's capacity for effective ULF vibration control under seismic conditions loads.

3. Jacket Platform with Nonlinear Vibration Isolation System

To verify the effectiveness of the proposed nonlinear X-shaped vibration isolation system for jacket offshore platforms, a real offshore platform (North Rankin B' (NRB')) [3] was selected for X-shaped vibration isolation system design and numerical analysis, as shown in Figure 9a. The NRB' platform is a major offshore gas platform located approximately 135 kilometers northwest of Dampier, Western Australia. The platform carries out jacket installation, platform hoisting and submarine pipeline laying in a water depth of 125 meters, representing the high technical level of offshore engineering at that time. It was primarily constructed to develop the low-pressure gas reserves of the Rankin field, which the original North Rankin A' (NRA') platform could no longer efficiently extract. The platform is physically connected to the NRA' platform by a 100-meter bridge, creating the integrated Rankin A'B' hub. This allows for shared utilities and accommodation. With a topsides weight of over 30,000 tons, NRB' can process up to 1.6 billion standard cubic feet of gas per day. For the convenience of simulation analysis, an idealized 3-DOF system is regarded as a simplified model of the platform by the model reduction method (as shown in Figure 9b). Table 1 lists some dynamic characteristics of the platform model, such as the stiffness of each layer and the lumped mass values.

The damping matrix for the NRB' platform is formulated using Rayleigh damping coefficients, derived from the modal damping ratios associated with the first two frequencies [3]. The damping ratios of the first three vibration modes are set to 0.05, 0.03, and 0.02, respectively [3]. Based on the simplified structural model of the jacket platform, the governing dynamic equation is given by,

$$[M]\{\ddot{x}\} + [C]\{\dot{x}\} + [K]\{x\} = -[M]\ddot{u}_g \quad (14)$$

 doi:10.20944/preprints202510.0385.v1

Where, $[M]$, $[C]$ and $[K]$ are mass, damping and stiffness matrices of the simplified 3-DOF model, respectively; and $\{x\}$, $\{\dot{x}\}$ and $\{\ddot{x}\}$ are the vectors of displacement, velocity and acceleration of structural response, respectively. $\ddot{u}_g$ is the earthquake acceleration signal. According to the Equation (14), the displacement and acceleration of deck layer of NRB' platform can be calculated.

Table 1. Parameters of NRB' platform [3].

	Level1	Level2	Level3
Mass (ton)	9000 (m_1)	11000 (m_2)	31000 (m_3)
Stiffness (MN/m)	400 (k_1)	430 (k_2)	39 (k_3)

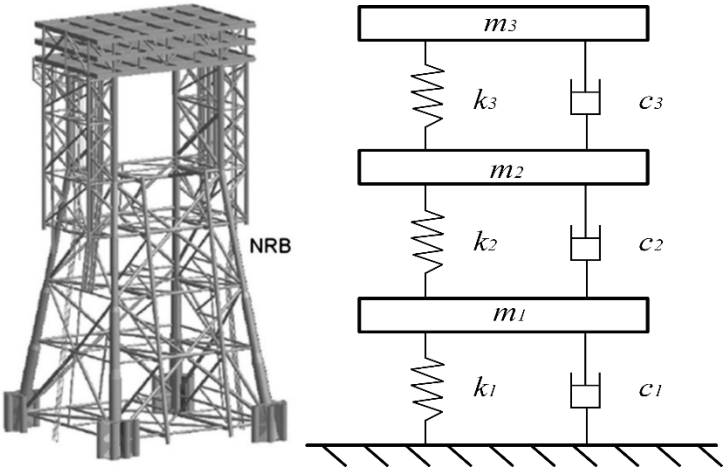

(a) Jacket structure diagram, (b) Simplified 3-DOF model.

Figure 9. The NRB' jacket offshore platform.

The proposed vibration isolation system for jacket offshore platforms places an NXVIS between the deck and the jacket structure of NRB' platform, as shown in Figure 10a. To avoid excessively increasing the overall height of the NRB' platform and thus introducing unforeseen risks, the bar length l of the X-shaped isolator is set to 0.75 m, which makes the height of the NXVIS only about 2m. The X-shaped isolator's primary function is to carry the upper load and achieve vibration isolation through nonlinear dynamic stiffness and damping. The structure of the X-shaped isolator is shown in Figure 10b. However, the X-shaped isolator corresponding to a bar length l of 0.75 m cannot bear the weight of the deck layer alone. Considering the weight of the deck and the QZS range of the system, 16 isolators were selected and evenly distributed in the nonlinear X-shaped isolation layer. Figure 10c shows the installation details of the X-shaped isolation layer. Figure 10c shows the installation details of the X-shaped isolation layer. As shown in Figure 10c, sixteen isolators are installed evenly between the jacket cap and the deck. This configuration results in the NXVIS being positioned between 16 and 18 m above the water surface. The X-shaped isolation layer not only isolates vibration transmission but also provides a compliant, localized deformation layer between the jacket structure and the deck, making the isolator in a QZS range. The validation of passive vibration isolation layers has been discussed previously [3,21]. Conventional vibration isolation approaches are frequently tailored to environmental load profiles. Consequently, their adaptability is generally deficient, and their efficacy in handling the intricacies of complex maritime environments—especially broadband excitations—remains limited. The proposed NXVIS can achieve ULF and wide-band vibration isolation under high loads, enabling the offshore platform to cope not only with low-frequency wave loads but also with wide-band seismic loads. The vibration isolation characteristics of the NXVIS have been verified in Section 2, demonstrating its effectiveness in reducing vibrations within the frequency band above 0.4 Hz. In addition, the NXVIS can dissipate

 doi:10.20944/preprints202510.0385.v1

vibration energy through its damping properties. Although low-frequency wave loads constantly cause platform vibration, seismic loads are the primary threat to platform safety, especially for jacket offshore platforms located in seismic zones. Therefore, this study focuses on vibration control of jacket offshore platforms under seismic loads.

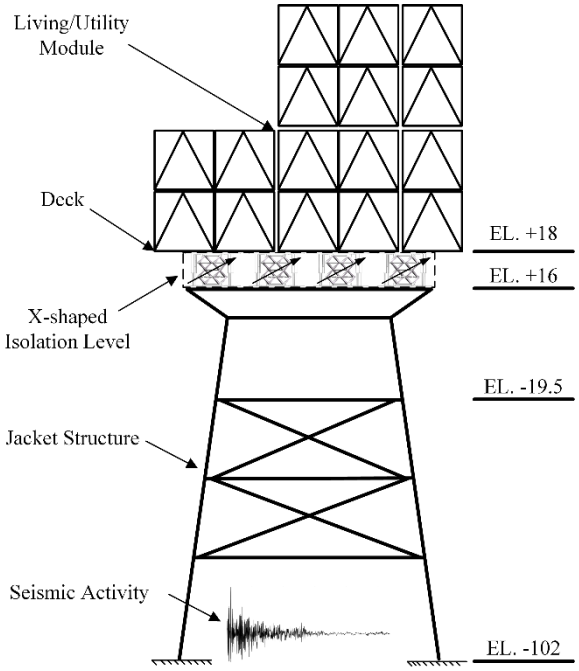

(a) The jacket offshore platforms with the NXVIS.

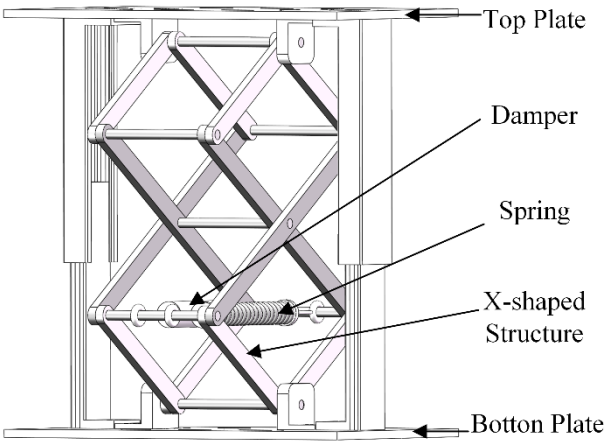

(b) Schematics of X-shaped isolator.

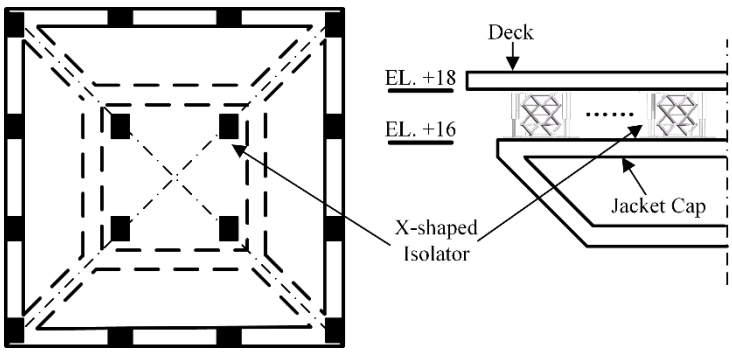

(c) Schematic diagram of the X-shaped isolation layer.

 doi:10.20944/preprints202510.0385.v1

Figure 10. Nonlinear X-shaped vibration isolation system.

Based on the dynamic characteristics of the NRB' platform and the designed NXVIS, a simplified 3-DOF platform with NXVIS is shown in Figure 11. In this figure, K_{Non} and C_{Non} are the dynamic stiffness and damping related to the relative displacement between layers, which can be expressed as,

$$K_{Non}\left(x_3-x_2\right)=\varepsilon_0+\varepsilon_1\left(x_3-x_2\right)+\varepsilon_2\left(x_3-x_2\right)^2+\varepsilon_3\left(x_3-x_2\right)^3 \quad (15)$$

$$C_{Non}\left(x_3-x_2\right)=\varepsilon_4+\varepsilon_5\left(x_3-x_2\right)+\varepsilon_6\left(x_3-x_2\right)^2+\varepsilon_7\left(x_3-x_2\right)^3 \quad (16)$$

Where, x_2 and x_3 are the absolute displacements of the second and third layers of the NRB' platform, respectively. The coefficients $\varepsilon_0-\varepsilon_7$ are listed in the "Appendix B". The Taylor expansion coefficients can be obtained from Appendix B. Since the NXVIS has strong nonlinearity, the Lagrangian method is used to solve the dynamic equation of the simplified 3-DOF platform with NXVIS. The nonlinear dynamic equation of the NRB' platform with NXVIS (as shown in Figure 11) can be written as,

$$m_1\ddot{x}_1+\left(c_1+c_2\right)\dot{x}_1-c_2\dot{x}_2+\left(k_1+k_2\right)x_1-k_2x_2=-m_1\ddot{u}_g \quad (17)$$

$$m_2\ddot{x}_2+c_2\left(\dot{x}_2-\dot{x}_1\right)-\frac{c_0\left(l\sin\alpha+\frac{x_3-x_2}{2n}\right)^2\left(\dot{x}_3-\dot{x}_2\right)}{n^2\sqrt{l^2-\left(l\sin\alpha+\left(x_3-x_2\right)/2n\right)^2}}+k_2\left(x_2-x_1\right)$$
$$-\frac{k_0\left(l\sin\alpha+\frac{x_3-x_2}{2n}\right)\left(2l\cos\alpha-2\sqrt{l^2-\left(l\sin\alpha+\left(x_3-x_2\right)/2n\right)^2}-y_s\right)}{n\sqrt{l^2-\left(l\sin\alpha+\left(x_3-x_2\right)/2n\right)^2}}=-m_2\ddot{u}_g \quad (18)$$

$$m_3\ddot{x}_3+\frac{c_0\left(l\sin\alpha+\frac{x_3-x_2}{2n}\right)^2\left(\dot{x}_3-\dot{x}_2\right)}{n^2\sqrt{l^2-\left(l\sin\alpha+\left(x_3-x_2\right)/2n\right)^2}}+$$
$$\frac{k_0\left(l\sin\alpha+\frac{x_3-x_2}{2n}\right)\left(2l\cos\alpha-2\sqrt{l^2-\left(l\sin\alpha+\left(x_3-x_2\right)/2n\right)^2}-y_s\right)}{n\sqrt{l^2-\left(l\sin\alpha+\left(x_3-x_2\right)/2n\right)^2}}+m_3g=-m_3\ddot{u}_g \quad (19)$$

Where, m_i, k_i and c_i are NRB' platform mass, stiffness and damping coefficient of the ith floor (i=1-3), respectively. x_i represents the displacement of the ith floor relative to ground motion, respectively. k_0 and c_0 are the stiffness and damping coefficient of the proposed X-shaped anti-vibration structure respectively, and their values can be found in Appendix A. It is important to note that k_0 and c_0 are not the stiffness and damping coefficient of NXVIS. They are only the stiffness and damping coefficient of the spring and damper in NXVIS. The real stiffness and damping coefficients of NXVIS are the dynamic stiffness and damping coefficients determined by the relative displacements x_2 and x_3 between layers, which can be found in Equations (15) and (16). In addition, the gravity term in Equation (19) cancels out the elastic force in the spring caused by gravity. Therefore, the dynamic response of the structure will still fluctuate around the static equilibrium position (zero position). The values of the remaining parameters are provided in Appendix A.

 doi:10.20944/preprints202510.0385.v1

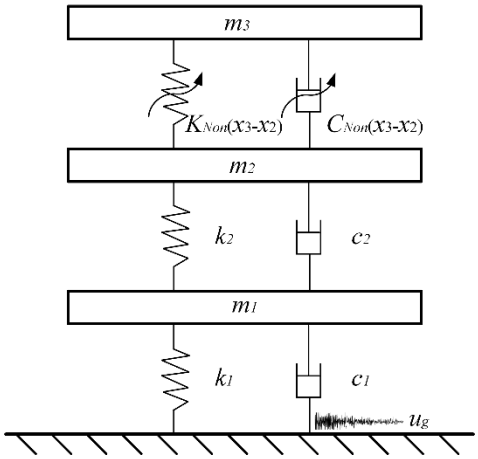

Figure 11. The NRB' platform with NXVIS.

4. Results and Discussions

To fully validate the effectiveness of the proposed NXVIS, the NRB' platform in Western Australia was selected for numerical analysis, which is a very important and representative offshore natural gas production platform. Similarly, to ensure the objectivity of the numerical analysis results, two typical seismic loads (El Centro, 1940; Taft, 1952) were considered, as shown in Figures 12 and 13.

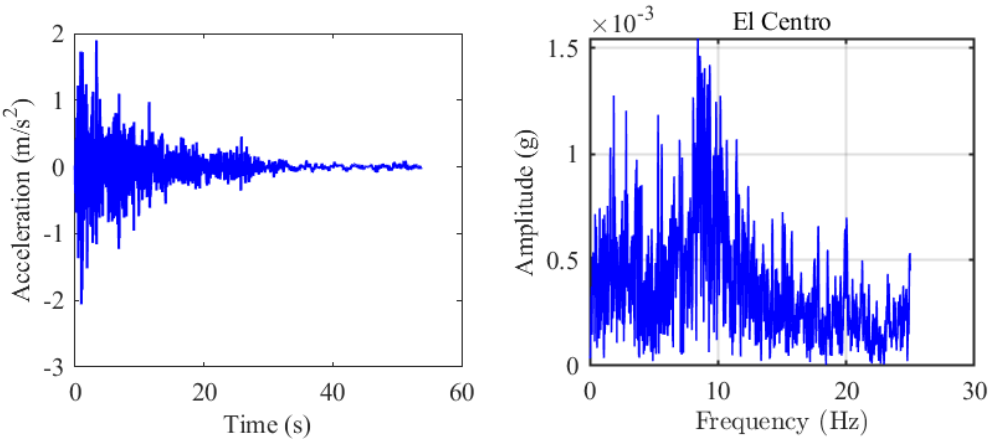

(a) Time domain, (b) Frequency domain.

Figure 12. El Centro seismic load.

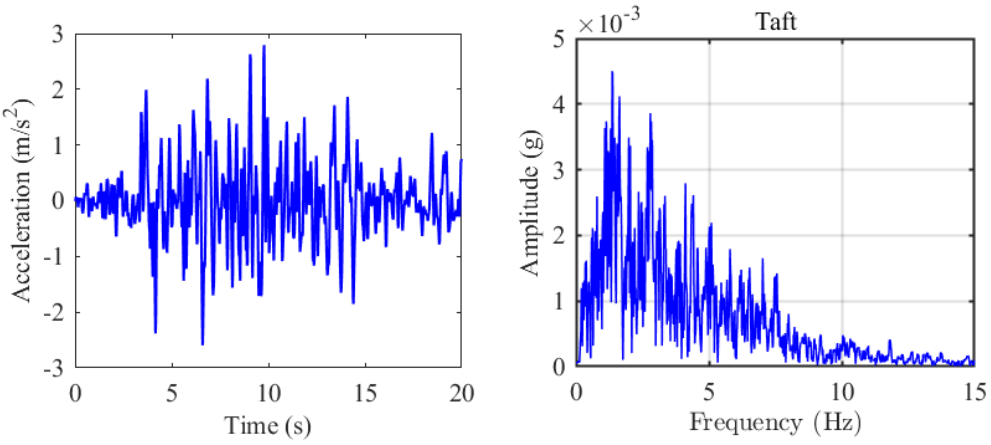

(a) Time domain, (b) Frequency domain.

 doi:10.20944/preprints202510.0385.v1

Figure 13. Taft seismic load.

Figure 12 shows the Imperial Valley earthquake of May 18, 1940, known as the El Centro earthquake. It is one of the most famous and widely used seismic loads in the world and is a very representative example. Figure 12a shows that the seismic signal initially has concentrated energy and a large response amplitude, but the energy gradually decays over time. Figure 12b shows the El Centro earthquake in the frequency domain. The earthquake has two frequency peaks, at 1.88 Hz and 8.43 Hz, with the major energy concentrated between 1.0 Hz and 10.0 Hz. This indicates that larger earthquakes release more low-frequency energy, and vibration control for jacket offshore platforms should primarily address these extreme seismic loads.

Figure 13 shows the seismic acceleration recorded at a seismic station in Taft, California, during the 1952 Kern County earthquake, known as the Taft earthquake. It is one of the earliest fully documented strong earthquake records in the world. Due to its high data quality and typical characteristics, it has become a standard seismic load recognized by international society, widely used in seismic performance testing of structures such as buildings, bridges, and nuclear power plants. Unlike the El Centro earthquake, the Taft seismic load exhibits a strong response throughout the entire period. As shown in Figure 13b, the Taft seismic load peaks at 1.38 Hz, with most of its energy concentrated between 0.8 Hz and 5.0 Hz.

These two types of seismic loads are highly representative, characteristic, and widely applicable, and therefore can well reflect the effectiveness of vibration isolation solutions. Based on these two typical seismic loads and the dynamic model of an NRB' offshore platform with an X-shaped anti-vibration structure, a numerical analysis of the offshore platform's vibration performance was conducted. The deck is a crucial area of offshore platforms for oil and gas production and crew life. The displacement response of the deck can cause structural fatigue damage and equipment damage, and in severe cases, even cause the platform to capsize, resulting in significant losses. The acceleration response of the deck can affect staff comfort and the operation of sensitive equipment, ultimately impacting production efficiency and worker health. Therefore, this study focuses on analyzing the structural response of the deck. The results are presented in Figures 14 and 15. It should be clarified that the "Original" denotes the NRB' platform without any anti-vibration mechanisms, while the "Isolation" refers specifically to the platform integrated with the NXVIS.

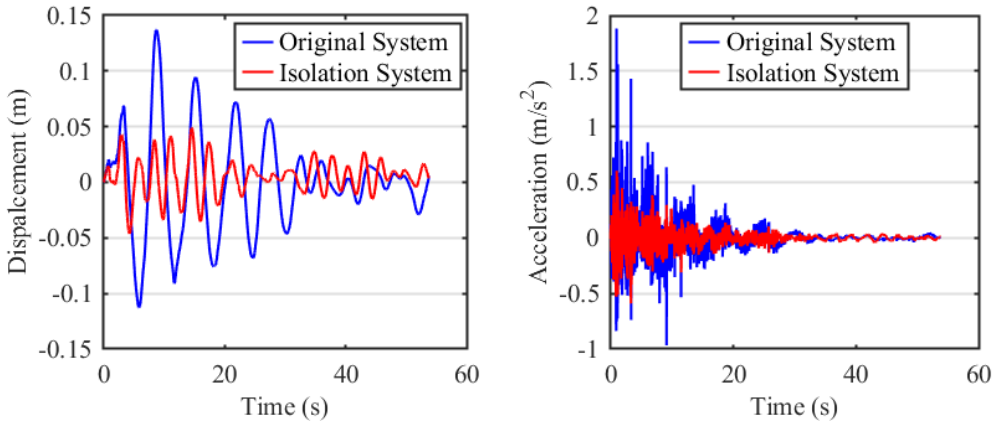

(a) Deck displacement, (b) Deck acceleration.

Figure 14. Dynamic response time histories of the NRB platform deck under El Centro seismic excitation.

 doi:10.20944/preprints202510.0385.v1

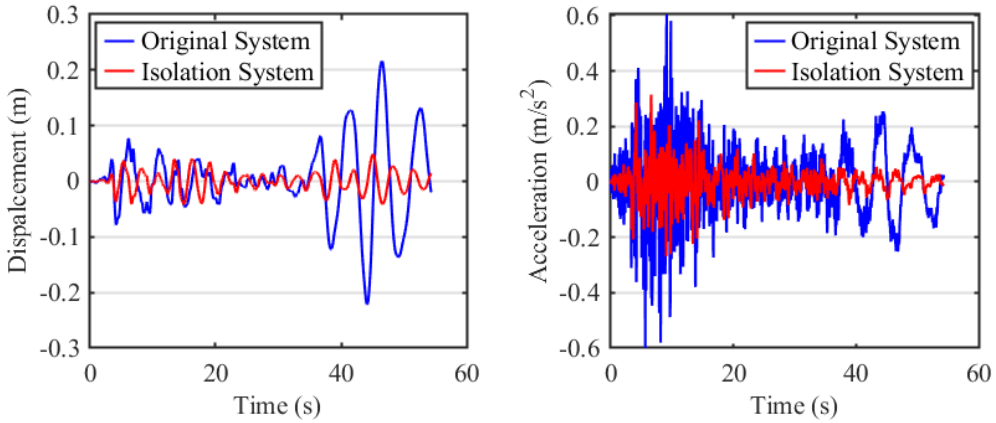

(a) Deck displacement, (b) Deck acceleration.

Figure 15. Dynamic response time histories of the NRB platform deck under Taft seismic excitation.

Figures 14 and 15 show that the NRB' jacket offshore platform equipped with a NXVIS can significantly reduce the displacement and acceleration response of the deck under seismic loads. Figure 14 shows the displacement and acceleration response of the deck under the El Centro earthquake load. The maximum displacements of the deck with and without the NXVIS are 4.9 cm and 13.7 cm respectively, reduction by 64.23%. The peak deck accelerations were measured at 0.602 m/s² and 1.883 m/s², corresponding to a significant reduction of 68.03%. Figure 15 presents the displacement and acceleration time histories of the deck subjected to Taft seismic excitation. The peak deck displacements with and without the NXVIS were measured at 4.9 cm and 21.6 cm respectively, corresponding to a significant reduction of 77.31%. The peak deck accelerations reached 0.315 m/s² and 0.604 m/s², representing a substantial reduction of 47.85%. This demonstrates that the NXVIS can achieve effective vibration reduction within the seismic frequency band by changing the system's natural frequency. For quantitative comparison, Table 2 lists the maximum, minimum, and RMS values of the performance indicators under different systems (original system and isolation system) and seismic loads (El Centro Earthquake; Taft Earthquake).

Table 2. Deck layer responses under different systems.

	Index	Original	Isolation	Reduction %
El Centro	Max(Dis.)	0.137 m	0.049 m	64.23
	Min(Dis.)	-0.112 m	-0.046 m	58.93
	RMS(Dis.)	0.045 m	0.019 m	57.78
	Max(Acc.)	1.883 m/s²	0.602 m/s²	68.03
	Min(Acc.)	-0.966 m/s²	-0.590 m/s²	38.92
	RMS(Acc.)	0.145 m/s²	0.098 m/s²	32.41
Taft	Max(Dis.)	0.216 m	0.049 m	77.31
	Min(Dis.)	-0.222 m	-0.042 m	81.08
	RMS(Dis.)	0.068 m	0.018 m	73.53
	Max(Acc.)	0.604 m/s²	0.315 m/s²	47.85
	Min(Acc.)	-0.600 m/s²	-0.269 m/s²	55.17
	RMS(Acc.)	0.128 m/s²	0.06 m/s²	53.12

As shown in Table 2, compared to offshore platforms without NXVIS, offshore platforms equipped with NXVIS significantly reduce deck vibration response under seismic loads, with the maximum reduction reaching 81.08%. Under seismic excitation from both the El Centro and Taft records, the NXVIS achieved substantial reductions in the root mean square (RMS) deck acceleration values, amounting to 32.41% and 53.12%, respectively. Deck acceleration serves as a critical metric for assessing the vibrational performance of marine vessels and offshore structures, with direct

 doi:10.20944/preprints202510.0385.v1

implications for crew comfort, as well as the operational safety and reliability of sensitive on-board equipment. Notably, under both loading scenarios, the peak, minimum, and RMS acceleration values of the deck equipped with the NXVIS were consistently reduced compared to the original platform, confirming the system's superior vibration suppression performance. The minimum deck acceleration under both load conditions was reduced by 32.41% and 53.12%, respectively. This is because the natural mode of the original NRB' platform is closer to the main earthquake frequency band, making it more susceptible to resonance. However, the offshore platform with the NXVIS can dynamically adjust the system stiffness, achieving effective vibration isolation within the external excitation frequency band, thereby effectively suppressing the vibration response.

It should also be noted that the system stiffness of the isolation layer is relatively low, which generally reduces the acceleration response while increasing the relative motion between deck and jacket structure. This increase in relative displacement may affect the stability of equipment installation and system durability. However, the offshore platform with the NXVIS significantly reduces the relative displacement of the structure while maintaining better acceleration control. This is because nonlinear systems can achieve HSLDS characteristics. For example, under two seismic loads, the RMS value of the deck displacement was reduced by 57.78% and 73.53%, respectively, demonstrating the significant advantage of this control strategy in improving overall stability. This outcome further verifies that the proposed nonlinear isolation approach successfully reconciles the response interplay between acceleration and displacement while surpassing conventional linear passive isolation methods in overall vibration suppression effectiveness, highlighting its potential for practical deployment in offshore platform vibration mitigation.

5. Conclusions

This paper proposes a biomimetic nonlinear X-shaped vibration isolation system, inspired by the X-shaped supporting structure of the human leg, to mitigate vibrations of jacket offshore platforms under the action of seismic loads. The NXVIS demonstrates superior tunable stiffness, adaptive damping characteristics, and high load-bearing capacity, with all three properties being programmable through strategic configuration of its structural parameters. To verify the effectiveness of the proposed nonlinear X-shaped vibration isolation system for vibration control of offshore platform under the action of seismic loads, theoretical and numerical analyses were conducted on the dynamic response of the NRB' offshore platform located in the waters of Western Australia under two typical seismic loads. The principal findings of this study can be summarized as follows:

1. System modeling and theoretical analysis demonstrate that the NXVIS exhibits distinct nonlinear quasi-zero stiffness, nonlinear damping, and high load capacity, enabling ULF with minimal peak values and high vertical load capacity. This design provides tunable load-bearing and frequency response characteristics—a significant advantage over traditional passive isolation methods—allowing precise adaptation to specific platform requirements and complex marine loading scenarios.

2. By modulating key structural parameters, including bar length and spring stiffness, the system can be tuned to exhibit diverse nonlinear stiffness profiles and a broad QZS operating range. This characteristic enables ULF vibration suppression without compromising the structural load-bearing integrity.

3. Under typical earthquake loads, the offshore platform equipped with the NXVIS significantly reduced the dynamic response of the offshore platform. Under the El Centro earthquake load, the maximum deck acceleration of the platform with the X-shaped vibration isolation system was reduced by 68.03%, and the maximum deck displacement was reduced by 64.23% compared to the original system. Under the Taft earthquake load, the maximum deck acceleration and displacement were reduced by 77.31% and 47.85%, respectively.

4. Due to the HSLDS characteristic of the X-shaped nonlinear isolator, the proposed NXVIS can effectively suppress the deck acceleration response of the offshore platform with small deck

 doi:10.20944/preprints202510.0385.v1

displacements, ensuring structural stability. The results demonstrate that the proposed NXVIS effectively ensures structural safety and provides good comfort.

It is worth emphasizing that the NXVIS is highly flexible in terms of size and load capacity, and its manufacturing and vibration isolation applications are also extremely cost-effective. These outstanding properties and intrinsic nonlinear characteristics make the proposed system an innovative solution for vibration control in jacket-type offshore platforms, providing a novel approach that extends beyond conventional structural vibration mitigation strategies. This system holds significant potential for widespread engineering application, promising considerable advantages across various industrial practices.

Author Contributions: Conceptualization, data curation, investigation, methodology, validation, writing—original draft preparation, Zhenghan Zhu; writing—review and editing, supervision, Yangmin Li. All authors have read and agreed to the published version of the manuscript.

Funding: This research was funded by the Research Impact Fund of Hong Kong (Grant No. R5047-22).

Data Availability Statement: Data is contained within the article.

Institutional Review Board Statement: Not applicable.

Informed Consent Statement: Not applicable.

Conflicts of Interest: The authors declare no conflict of interest.

Appendix A

Table A1. Parameters of the X-shaped isolator.

Parameters	Values
Mass1 M	1940 ton
Stiffness k	100 MN/m
Damping coefficient c	300 MNs/m
Bar length l	0.75 m
Angle α	43 deg
Angle β	63 deg
Layers number n	2.0

Appendix B

$$\varepsilon_0 = -\frac{y_s \tan\alpha}{n} \quad \text{(b.1)}$$

$$\varepsilon_1 = \frac{-y_s \sec^3\alpha + 2l\tan^2\alpha}{2ln^2} \quad \text{(b.2)}$$

$$\varepsilon_2 = \frac{3\left(-y_s + 2l\cos\alpha\right)\sec^4\alpha\tan\alpha}{8l^2n^3} \quad \text{(b.3)}$$

$$\varepsilon_3 = -\frac{\left(-y_s + 2l\cos\alpha\right)\left(-3 + 2\cos\left(2\alpha\right)\right)\sec^7\alpha}{16l^3n^4} \quad \text{(b.4)}$$

$$\varepsilon_4 = \frac{\tan\alpha}{n} \quad \text{(b.5)}$$

$$\varepsilon_5 = \frac{\sec^3\alpha}{2ln^2} \quad \text{(b.6)}$$

$$\varepsilon_6 = \frac{3\sec^4\alpha\tan\alpha}{8l^2n^3} \quad \text{(b.7)}$$

 doi:10.20944/preprints202510.0385.v1

$$\varepsilon_7 = -\frac{\left(-3+2\cos\left(2\alpha\right)\right)\sec^7\alpha}{16l^3n^4} \quad \text{(b.8)}$$

References

1. Zhang, Y.; Ma, H.; Xu, J.; Su, H.; Zhang, J. Model Reference Adaptive Vibration Control of an Offshore Platform Considering Marine Environment Approximation. *J. Mar. Sci. Eng.* **2023**, *11*, 138, doi:10.3390/jmse11010138.
2. Kandasamy, R.; Cui, F.; Townsend, N.; Foo, C.C.; Guo, J.; Shenoi, A.; Xiong, Y. A Review of Vibration Control Methods for Marine Offshore Structures. *Ocean Eng.* **2016**, *127*, 279–297, doi:10.1016/j.oceaneng.2016.10.001.
3. Leng, D.; Zhu, Z.; Xu, K.; Li, Y.; Liu, G. Vibration Control of Jacket Offshore Platform through Magnetorheological Elastomer (MRE) Based Isolation System. *Appl. Ocean Res.* **2021**, *114*, 102779, doi:10.1016/j.apor.2021.102779.
4. Zhang, Y.; Ma, H.; Xu, J. Neural Network-Based Fuzzy Vibration Controller for Offshore Platform with Random Time Delay. *Ocean Eng.* **2021**, *225*, 108733, doi:10.1016/j.oceaneng.2021.108733.
5. Som, A.; Das, D. Seismic Vibration Control of Offshore Jacket Platforms Using Decentralized Sliding Mode Algorithm. *Ocean Eng.* **2018**, *152*, 377–390, doi:10.1016/j.oceaneng.2018.01.013.
6. Hosseini Lavassani, S.H.; Mousavi Gavgani, S.A.; Doroudi, R. Optimal Control of Jacket Platforms Vibrations under the Simultaneous Effect of Waves and Earthquakes Considering Fluid-Structure Interaction. *Ocean Eng.* **2023**, *280*, 114593, doi:10.1016/j.oceaneng.2023.114593.
7. Sardar, R.; Chakraborty, S. Wave Vibration Control of Jacket Platform by Tuned Liquid Dampers. *Ocean Eng.* **2022**, *247*, 110721, doi:10.1016/j.oceaneng.2022.110721.
8. Hussan, M.; Rahman, M.S.; Sharmin, F.; Kim, D.; Do, J. Multiple Tuned Mass Damper for Multi-Mode Vibration Reduction of Offshore Wind Turbine under Seismic Excitation. *Ocean Eng.* **2018**, *160*, 449–460, doi:10.1016/j.oceaneng.2018.04.041.
9. Zheng, Z.; Chang, Z.; Zhao, L. Mitigating Deepwater Jacket Offshore Platform Vibration under Wave and Earthquake Loadings Utilizing Nonlinear Energy Sinks. *Ocean Eng.* **2023**, *283*, 115096, doi:10.1016/j.oceaneng.2023.115096.
10. Xu, T.; Li, Y.; Leng, D. Mitigating Jacket Offshore Platform Vibration under Earthquake and Ocean Waves Utilizing Tuned Inerter Damper. *Bull. Earthq. Eng.* **2023**, *21*, 1627–1650, doi:10.1007/s10518-022-01378-z.
11. Ou, J.; Long, X.; Li, Q.S.; Xiao, Y.Q. Vibration Control of Steel Jacket Offshore Platform Structures with Damping Isolation Systems. *Eng. Struct.* **2007**, *29*, 1525–1538, doi:10.1016/j.engstruct.2006.08.026.
12. Leng, D.; Zhu, Z.; Liu, G.; Li, Y. Neuro Fuzzy Logic Control of Magnetorheological Elastomer Isolation System for Vibration Mitigation of Offshore Jacket Platforms. *Ocean Eng.* **2022**, *253*, 111293, doi:10.1016/j.oceaneng.2022.111293.
13. Chen, D.; Huang, S.; Huang, C.; Liu, R.; Ouyang, F. Passive Control of Jacket–Type Offshore Wind Turbine Vibrations by Single and Multiple Tuned Mass Dampers. *Mar. Struct.* **2021**, *77*, 102938, doi:10.1016/j.marstruc.2021.102938.
14. Pourzangbar, A.; Vaezi, M. Effects of Pendulum Tuned Mass Dampers on the Dynamic Response of Jacket Platforms. *Ocean Eng.* **2022**, *249*, 110895, doi:10.1016/j.oceaneng.2022.110895.
15. Vaezi, M.; Pourzangbar, A.; Fadavi, M.; Mousavi, S.M.; Sabbahfar, P.; Brocchini, M. Effects of Stiffness and Configuration of Brace-Viscous Damper Systems on the Response Mitigation of Offshore Jacket Platforms. *Appl. Ocean Res.* **2021**, *107*, 102482, doi:10.1016/j.apor.2020.102482.
16. Jiang, K.; Li, H.; Lv, G.; Wang, L.; Wang, L.; Yu, H. Vibration Control of Deepwater Offshore Platform Using Viscous Dampers Under Wind, Wave, and Earthquake. *J. Mar. Sci. Eng.* **2025**, *13*, 1197, doi:10.3390/jmse13071197.
17. Cui, F.; Chen, S.; Hao, H.; Han, C.; Ni, R.; Zhuo, Y. Assessment of Hydrodynamic Performance and Motion Suppression of Tension Leg Floating Platform Based on Tuned Liquid Multi-Column Damper. *J. Mar. Sci. Eng.* **2024**, *12*, 328, doi:10.3390/jmse12020328.

18. Ghasemi, M.R.; Shabakhty, N.; Enferadi, M.H. Vibration Control of Offshore Jacket Platforms through Shape Memory Alloy Pounding Tuned Mass Damper (SMA-PTMD). *Ocean Eng.* **2019**, *191*, 106348, doi:10.1016/j.oceaneng.2019.106348.
19. Liu, S.; Yin, X.; Li, H.; Yang, J.; Li, P.; Li, P. Effectiveness of MTMD for Jacket Offshore Platform under Wave and Earthquake Excitations. *Soil Dyn. Earthq. Eng.* **2025**, *199*, 109654, doi:10.1016/j.soildyn.2025.109654.
20. Hokmabady, H.; Mohammadyzadeh, S.; Mojtahedi, A. Suppressing Structural Vibration of a Jacket-Type Platform Employing a Novel Magneto-Rheological Tuned Liquid Column Gas Damper (MR-TLCGD). *Ocean Eng.* **2019**, *180*, 60–70, doi:10.1016/j.oceaneng.2019.03.055.
21. Zhu, Z.; Wang, Y.; Wang, Y.; Jing, X. Nonlinear Inertia and Its Effect within an X-Shaped Mechanism – Part I: Modelling & Nonlinear Properties. *Mech. Syst. Signal Process.* **2023**, *200*, 110590, doi:10.1016/j.ymssp.2023.110590.
22. Jing, X. The X-Structure/Mechanism Approach to Beneficial Nonlinear Design in Engineering. *Appl. Math. Mech.* **2022**, *43*, 979–1000, doi:10.1007/s10483-022-2862-6.
23. Bian, J.; Jing, X. Superior Nonlinear Passive Damping Characteristics of the Bio-Inspired Limb-like or X-Shaped Structure. *Mech. Syst. Signal Process.* **2019**, *125*, 21–51, doi:10.1016/j.ymssp.2018.02.014.
24. Chai, Y.; Jing, X.; Chao, X. X-Shaped Mechanism Based Enhanced Tunable QZS Property for Passive Vibration Isolation. *Int. J. Mech. Sci.* **2022**, *218*, 107077, doi:10.1016/j.ijmecsci.2022.107077.
25. Feng, X.; Jing, X. Human Body Inspired Vibration Isolation: Beneficial Nonlinear Stiffness, Nonlinear Damping & Nonlinear Inertia. *Mech. Syst. Signal Process.* **2019**, *117*, 786–812, doi:10.1016/j.ymssp.2018.08.040.
26. Chen, S.; Xuan, M.; Xin, J.; Liu, Y.; Gu, S.; Li, J.; Zhang, L. Design and Experiment of Dual Micro-Vibration Isolation System for Optical Satellite Flywheel. *Int. J. Mech. Sci.* **2020**, *179*, 105592, doi:10.1016/j.ijmecsci.2020.105592.
27. Yang, J.; Ning, D.; Sun, S.S.; Zheng, J.; Lu, H.; Nakano, M.; Zhang, S.; Du, H.; Li, W.H. A Semi-Active Suspension Using a Magnetorheological Damper with Nonlinear Negative-Stiffness Component. *Mech. Syst. Signal Process.* **2021**, *147*, 107071, doi:10.1016/j.ymssp.2020.107071.
28. Zhou, H.; Gao, J.; Chen, Y.; Shen, Z.; Lv, H.; Sareh, P. A Quasi-Zero-Stiffness Vibration Isolator Inspired by Kresling Origami. *Structures* **2024**, *69*, 107315, doi:10.1016/j.istruc.2024.107315.
29. Ding, B.; Li, X.; Chen, S.-C.; Li, Y. Modular Quasi-Zero-Stiffness Isolator Based on Compliant Constant-Force Mechanisms for Low-Frequency Vibration Isolation. *J. Vib. Control* **2024**, *30*, 3006–3020, doi:10.1177/10775463231188160.
30. Leng, D.; Lv, P.; Zhu, Z.; Li, Y.; Liu, G. Experimental Study on Semi-Active Magnetorheological Elastomer Based Isolation System for Offshore Platform Using Wave Tank. *Ocean Eng.* **2024**, *292*, 116467, doi:10.1016/j.oceaneng.2023.116467.